Journal of Molecular Structure 1137 (2017) 615–625

Contents lists available at ScienceDirect

Journal of Molecular Structure

journal homepage: http://www.elsevier.com/locate/molstruc

Three oxime ether derivatives: Synthesis, crystallographic study, electronic structure and molecular electrostatic potential calculation

Tanusri Dey [a], Koduru Sri Shanthi Praveena [b], Sarbani Pal [b], Alok Kumar Mukherjee [a, *]

[a] Department of Physics, Jadavpur University, Kolkata 700032, India
[b] Department of Chemistry, MNR Degree and PG College, Kukatpally, Hyderabad 500085, India

ARTICLE INFO

Article history:
Received 18 October 2016
Received in revised form
17 January 2017
Accepted 23 February 2017
Available online 24 February 2017

Keywords:
Oxime ether derivative
X-ray powder diffraction
Hirshfeld surface analysis
Molecular electrostatic potential
Electronic structure

ABSTRACT

Three oxime ether derivatives, (*E*)-3-methoxy-4-(prop-2-ynyloxy)-benzaldehyde-*O*-prop-2-ynyl-oxime ($C_{14}H_{13}NO_3$) (**2**), benzophenone-*O*-prop-2-ynyl-oxime ($C_{16}H_{13}NO$) (**3**) and (*E*)-2-chloro-6-methylquinoline-3-carbaldehyde-*O*-prop-2-ynyl-oxime ($C_{14}H_{11}ClN_2O$) (**4**), have been synthesized and their crystal structures have been determined. The DFT optimized molecular geometries in **2**–**4** agree closely with those obtained from the crystallographic study. An interplay of intermolecular C–H···O, C–H···N, C–H···Cl and C–H···π(arene) hydrogen bonds and π···π interactions assembles molecules into a 2D columnar architecture in **2**, a 1D molecular ribbon in **3** and a 3D framework in **4**. Hirshfeld surface analysis showed that the structures of **2** and **3** are mainly characterized by H···H, H···C and H···O contacts but some contribution of H···N and H···Cl contacts is also observed in **4**. Hydrogen-bond based interactions in **2**–**4** have been complemented by calculating molecular electrostatic potential (MEP) surfaces. The electronic structures of molecules reveal that the estimated band gap in **3**, in which both aldehyde hydrogen atoms of formaldehyde-*O*-prop-2-ynyl-oxime (**1**) have been substituted by two benzene rings, is higher than that of **2** and **4** with only one aldehyde hydrogen atom replaced.

1. Introduction

Intermolecular interactions, in particular, hydrogen bonds, have been a topic of considerable importance due to their role in crystal engineering and biological recognition process [1–3]. Many of the synthons identified in supramolecular chemistry involve N/O–H···O/N hydrogen bonds, which provide the required selectivity and directionality to control molecular aggregation [4,5]. In addition to these relatively strong hydrogen bonds, weak interactions such as, C-H … X (X = O, N, Cl), C-H … π and π … π stacking are also important in describing the self-assembly process in molecular solids [6,7]. Single crystal X-ray diffraction (SXRD) is generally the method of choice for determining crystal structures of molecular compounds and the study of intermolecular interactions in the solid state has focused on geometrical criteria such as, D(donor) … A(acceptor) distance and D-H … A angle that can be directly measured from the SXRD analysis [8,9]. With recent advances in the direct space approaches for structure solution [10–13], *ab-initio* crystal structure determination from powder X-ray diffraction (PXRD) has been reported for organic systems with considerable molecular flexibility [14–17]. It should, however, be noted that structural crystallography with PXRD is significantly more challenging than that of its single crystal counterpart [18] because, first, the information content of a powder diffractogram is markedly lower, and second, it is far more difficult to extract structural information from a PXRD pattern due to systematic as well as random overlapping of peaks. This is reflected in the Cambridge Structural Database (version 5.37, update 2, CSD 2015 release) [19] search conducted among the organic compounds, which revealed that out of total 350196 entries only 1842 (~0.5%) structures have been solved from PXRD (including both laboratory and synchrotron X-ray data) without referring to an isotypic single crystal structure. Since structure determination from PXRD cannot establish the positions of hydrogen atoms unambiguously, consideration of geometrical criteria alone as obtained from the PXRD analysis without any supplementary evidence is unlikely to be reliable for assessing the hydrogen bonds. In this context, molecular electrostatic potential (MEP) [20–22] mapped onto a molecular surface can provide further insights into the nature of intermolecular interactions. This approach utilizes the calculated MEP surfaces around the molecule, in which the potential maxima and minima

* Corresponding author.
E-mail address: akm_ju@rediffmail.com (A.K. Mukherjee).

http://dx.doi.org/10.1016/j.molstruc.2017.02.089
0022-2860/

correspond to hydrogen bond donor and acceptor sites, respectively. Several attempts have been made relating MEP surfaces to crystal packing via intermolecular interactions [23–26].

In the current study we focus our attention to three oxime ether derivatives, (*E*)-3-methoxy-4-(prop-2-ynyloxy)-benzaldehyde-*O*-prop-2-ynyl oxime (**2**), benzophenone-*O*-prop-2-ynyl oxime (**3**) and (*E*)-2-chloro-6-methylquinoline-3-carbaldehyde-*O*-prop-2-ynyl oxime (**4**), modified by replacing the CH_2 group in formaldehyde-*O*-prop-2-ynyl oxime (**1**) (Scheme 1). Since our attempts to grow single crystals suitable for X-ray analysis resulted in assemblies of microcrystals, structure determination of **3** and **4** was accomplished from PXRD analysis. To examine the contribution and influence of intermolecular interactions on crystal packing, the Hirshfeld surfaces [27], associated 2D fingerprint plots [28] and enrichment ratios [29] have been calculated for the listed compounds and some related systems retrieved from the CSD. The intermolecular interactions in **2**–**4** have been correlated with the MEP surface analysis. The study also includes electronic structures of **2**–**4** via DFT calculations. It should be noted that the present contribution is the second example of propargyloxime aldehyde/ketone after 2-methyl-*N*-(prop-2-yn-1-yloxy)-5,6-dihydro-1,3-benzothiazol-7(4H)-imine (COWXET) [19], available in the CSD.

2. Experimental section

2.1. Materials and general methods

All chemicals were obtained from commercial sources. Solvents were dried using standard methods, and chromatographic purification was performed using silica gel (100–200 mesh). Elemental analysis was carried out with a Perkin-Elmer 240C elemental analyzer. Fourier-transform infrared (FTIR) spectra were measured as KBr pellets using a Perkin-Elmer RX1 spectrometer. ^{1}H and ^{13}C NMR spectra (300 MHz and 400 MHz) were recorded at 25 °C on a Varian-Gemini 300/400 MHz spectrometer using $CDCl_3$/DMSO-d_6 as solvent. Melting points were determined by open glass capillary method with a Sisco melting point apparatus and were uncorrected. Mass spectra were recorded on a HP 5989 instrument with electron ionization potential 70 eV. Reactions were monitored by thin layer chromatography (TLC) on pre-coated silica gel plates.

2.2. Synthesis

Primary oximes (**2b**, **3b** and **4b**) were synthesized by treating corresponding aldehydes (**2a** and **4a,** 1 mmol) or ketone (**3a**, 1 mmol) with hydroxyl amine hydrochloride (1.2 mmol) and sodium hydroxide (5 mmol) in ethanol (5 mL) at 25 °C followed by neutralization with acid. Crude oximes, thus obtained, were filtered and used without further purification. For the synthesis of compounds **2**, **3** and **4** (Scheme 2), equi-molar quantities of corresponding oximes (1 mmol of **2b**, **3b** and **4b**), anhydrous potassium carbonate (0.14 g, 1 mmol) and propargyl bromide (0.12 g, 1 mmol) were added to 15 mL of dry acetone and the resulting mixture was refluxed with vigorous magnetic stirring under anhydrous atmosphere. The progress of reaction was monitored by checking TLC at regular intervals. After completion of reaction, acetone was distilled out followed by addition of water and the compounds were extracted with ethyl acetate (3 × 15 mL). The combined organic extracts were washed with 25 mL brine solution and dried over anhydrous sodium sulphate. The crude products were purified by column chromatography to yield microcrystalline powders of (*E*)-3-methoxy-4-(prop-2-ynyloxy)-benzaldehyde-*O*-prop-2-ynyl oxime ($C_{14}H_{13}NO_3$) (**2**), benzophenone-*O*-prop-2-ynyl oxime ($C_{16}H_{13}NO$) (**3**) and (*E*)-2-chloro-6-methylquinoline-3-carbaldehyde-*O*-prop-2-ynyl oxime ($C_{14}H_{11}ClN_2O$) (**4**).

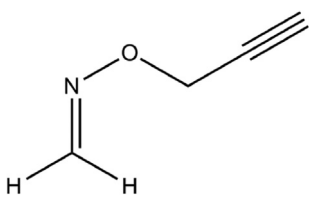

Scheme 1. Chemical diagram of formaldehyde *O*-prop-2-ynyl oxime (**1**).

2.3. Spectroscopic data

2.3.1. (E)-3-Methoxy-4-(prop-2-ynyloxy)-benzaldehyde-O-prop-2-ynyl oxime ($C_{14}H_{13}NO_3$) (**2**)

Colorless solid; yield 90%; mp 91(1) °C; mass (*m*/*z*) 243 (M+, 100%); ^{1}H NMR (400 MHz, $CDCl_3$): δ 8.07 (s, 1H), 7.27 (d, *J* 1.8 Hz, 1H), 7.06–7.00 (m, 2H), 4.79 (d, *J* 2.2 Hz, 2H), 4.77 (d, *J* 2.2 Hz, 2H), 3.93 (s, 3H), 2.54 (t, *J* 2.2 Hz, 1H), 2.52 (t, *J* 2.2 Hz, 1H); ^{13}C NMR (100 MHz, DMSO-d_6): δ 149.7, 149.2, 148.3, 124.9, 120.9, 113.5, 109.0, 80.2, 78.9, 78.5, 77.4, 61.1, 55.9, 55.4; elemental analysis: found C 69.25, H 5.40, N 5.69%, calculated for $C_{14}H_{13}NO_3$: C 69.13, H 5.36, N 5.76%.

2.3.2. Benzophenone-O-prop-2-ynyl oxime ($C_{16}H_{13}NO$) (**3**)

Colorless solid; yield 98%; mp 61(1) °C; mass (*m*/*z*) 236 (M+, 100%); ^{1}H NMR (400 MHz, $CDCl_3$): δ 7.51–7.49 (m, 2H), 7.44–7.41 (m, 3H), 7.39–7.25 (m, 5H), 4.76 (d, *J* 2.4 Hz, 2H), 2.46 (t, *J* 2.4 Hz, 1H), ^{13}C NMR (100 MHz, $CDCl_3$): δ 158.3, 136.1, 132.9, 129.6, 129.0, 128.3, 80.0, 74.4, 61.9, IR (KBr) ν_{max}/cm^{-1}: 3283, 3063, 3029, 2919, 1493, 1444, 1424, 1355, 1328, 1053, 1003, 967, 922, 862, 773, 692; elemental analysis: found C 81.52, H 5.47, N 5.88%, calculated for $C_{16}H_{13}NO$: C 81.70, H 5.53, N 5.96%.

2.3.3. (E)-2-Chloro-6-methylquinoline-3-carbaldehyde-O-prop-2-ynyl oxime ($C_{14}H_{11}ClN_2O$) (**4**)

Colorless solid; yield 93%; mp 125(1) °C; mass (*m*/*z*) 259 (M+, 100%); ^{1}H NMR (400 MHz, $CDCl_3$): δ 8.61 (s, 1H), 8.60 (s, 1H), 7.89 (d, *J* 8.4 Hz, 1H), 7.61 (d, *J* 10.8 Hz, 1H), 7.58 (d, *J* 2.0 Hz, 1H), 4.85 (d, *J* 2.4 Hz, 2H), 2.56 (t, *J* 2.4 Hz, 1H), 2.18 (s, 3H); ^{13}C NMR (100 MHz, $CDCl_3$): δ 148.0, 146.5, 146.4, 137.7, 135.3, 133.8, 127.9, 127.0, 126.8, 123.7, 79.1, 75.1, 62.2, 21.6, IR (KBr) ν_{max}/cm^{-1}: 3273, 3061, 2920, 1625, 1600, 1500, 1225, 1120, 830; elemental analysis: found C 64.91, H 4.19, N 10.88%, calculated for $C_{14}H_{11}ClN_2O$: C 65.00, H 4.26, N 10.83%.

2.4. Single crystal X-ray analysis of $C_{14}H_{13}NO_3$ (**2**)

Single crystal suitable for X-ray structure analysis was obtained by slow evaporation of a solution of **2** in a mixture of ethyl acetate and isopropyl alcohol (2:1). Intensity data were collected at 293(2) K on a Bruker Smart APEX II CCD area detector using graphite monochromated Mo Kα radiation(λ = 0.7107 Å). Data reduction was performed with SAINT [30] and an absorption correction was applied using SADABS [31]. The crystal structure was solved by direct methods with SHELXS97 [32] and refined using SHELXL97 [32] with anisotropic displacement parameters for all non-hydrogen atoms. The positions of hydrogen atoms were located from difference Fourier maps and refined with isotropic displacement parameters. The molecular view and crystal packing diagrams were generated using the Mercury (version 3.8) program [33]. Geometrical calculations were carried out with PLATON [34].